ADVANCED FUNCTIONAL MATERIALS
www.afm-journal.de

Protein-Engineered Elastin Fibers as Building Blocks for The Textile-Based Assembly of Tissue Equivalents

*Ikram El Maachi, Alexander Loewen, Sergio Acosta, Stephan Rütten, J. Carlos Rodríguez-Cabello, Stefan Jockenhoevel, and Alicia Fernández-Colino**

Native tissues feature unique hierarchical designs, in which fiber units are arranged from the bottom up in anisotropic patterns. The processing of biomaterials into fibers, followed by their textile-like assembly into complex patterns, is therefore a promising avenue to engineer native-like tissue replacements. Here it is shown for the first time the fabrication of meter-long hydrogel fibers prepared from engineered elastin using a microinjection system and exploiting the catalyst-free click chemistry. Given their similarity to native elastin, the fabricated elastin-like fibers achieved excellent stretching (500%) and recoiling performance. Moreover, the fabrication scheme is compatible with the implementation of a salt-leaching gas-foaming approach, resulting in highly porous elastin-like fibers (the first of their kind). From the translation perspective, the fibers can be autoclaved, which allows for sterilization and long-term storage. Human umbilical vein endothelial cells cultured on autoclaved fibers produced a confluent endothelial layer lining the fiber surface, in which the cells became aligned in response to physiological fiber stretching. It is also shown that these functional fibers can be assembled by weaving, braiding and knitting, with various spatial patterns. Overall, the elastin-like fibers can be used as building blocks for the reconstruction of functional tissues using the principles of textile technology.

1. Introduction

Nature builds from the bottom up, converting chemically simple building blocks into sophisticated structures[1,2] and native tissues are no exception to this construction strategy. Undoubtedly, nature has demonstrated its excellence as a designer. During billions of years of evolution, nature has shaped and refined the design of biological systems including functional, long-lasting tissues. The outstanding properties of native tissues lie on two different levels: the inherent characteristics of their materials and the arrangement of these materials in controlled hierarchical structures. The hierarchical structure of all tissues has one common element: the fiber. The ubiquity of fibrous proteins (e.g., collagen and elastin) in the native extracellular matrix (ECM) and their arrangement into higher-order net-like structures[3] means that fibers are the biomimetic building block of choice in tissue equivalents, highlighting the overlap between the fields of tissue engineering (TE) and textiles.[4,5]

The textile technologies have an history of over 30 000 years, thus encompassing well-established and standardized manufacturing techniques such as weaving, knitting and braiding, that are exploited for manufacturing daily items (clothes, filters), but also high value products (medical devices).[6] Textile technologies allow the development of 3D constructs with customized structures spanning multiple scales.[7] This requires precise control over various material properties, including the orientation of fibers and the size, shape, arrangement and density of pores, thus approximating the mechanical and functional

I. El Maachi, A. Loewen, S. Acosta, S. Jockenhoevel, A. Fernández-Colino
Department of Biohybrid & Medical Textiles (BioTex), AME –Institute of Applied Medical Engineering, Helmholtz Institute
RWTH Aachen University
52074 Aachen, Germany
E-mail: fernandez@ame.rwth-aachen.de

The ORCID identification number(s) for the author(s) of this article can be found under https://doi.org/10.1002/adfm.202313204

DOI: 10.1002/adfm.202313204

S. Rütten
Electron Microscopy Facility
Uniklinik RWTH Aachen
52074 Aachen, Germany

J. C. Rodríguez-Cabello
CIBER-BBN, Edificio LUCIA
CIBER-BBN, Edificio LUCIA
Universidad de Valladolid
Valladolid 47011, Spain

S. Jockenhoevel
AMIBM-Aachen-Maastricht-Institute for Biobased Materials
Maastricht University
Geleen 6167 RD, The Netherlands

characteristics of real tissues.[8–10] Thus far, such constructs have been deployed, with relative success, to provide physical support for prolapsed organs and surgical repairs[11–13] as well as for other load-bearing applications, including tendons as well as cardiovascular medical devices (vascular grafts,[14] heart valve sewing rings[15]). However, the implants are still based on synthetic materials such as polyethylene terephthalate, polylactic acid or polyglycolic acid,[16] which are strong and versatile but cannot recapitulate the genuine biochemical milieu required for effective tissue regeneration.[17] This can lead to suboptimal integration or even rejection following implantation, thereby creating a demand for a novel generation of yarns crafted from natural, biologically compatible materials.

Elastin is an essential component of native tissues, contributing significantly to their mechanical and bioactive functions.[18] For example, the absence of elastin in medical devices such as vascular implants can lead to stenotic and thrombotic events, culminating in device failure.[19] In contrast, incorporating elastin into a vascular replacement can enhance its performance in vivo due to the ability of elastin-based components to facilitate elastic contraction and expansion, promote rapid endothelialization, and prevent the over-proliferation of smooth muscle cells and platelet activation.[20,21] Artificial elastin, specifically elastin-like recombinamers (ELRs), represents an appealing solution for the production of tissue replacements with enhanced in vivo performance. ELRs are engineered protein polymers that combine the best of both worlds – the reproducibility of synthetic materials and the biocompatibility and bioactivity of biological ones.[22,23] These protein-engineered polymers can prevent fibrotic tissue formation and favor the proliferation of pro-healing type-2 macrophages over pro-inflammatory type-1 macrophages.[24,25]

The sequence of ELRs can be tailored to confer specific properties, thereby providing a versatile platform for the fabrication of cell-instructive TE scaffolds.[19,26] For instance, cell-binding motifs such as RGD, or protease-sensitive sequences (i.e., GTAR or DRIR) can be incorporated into their backbone to modulate cell migration and scaffold integration.[27] Additionally, ELRs can be chemically derivatized with catalyst-free click cross-linkable groups (e.g., azide groups), thus enabling the fabrication of stable 3D networks using catalyst-free click chemistry. This cutting-edge technology has been used to fabricate protein-engineered scaffolds with exceptional properties for tissue regeneration including the spatiotemporal control of angiogenesis and neurogenesis,[28] and the modulation of post-ischemic remodeling.[29] We have also fabricated elastin-based cell-free systems, in the form of vascular grafts,[30] heart valves,[31] and venous valves,[32] that withstand hydrodynamic conditions simulated in vitro.

One drawback of the examples described above is their reliance on top-to-bottom fabrication schemes, ultimately failing to fully implement and capitalize on the bottom-up principles inherent to natural tissues.[33] Here, for the first time, we use these advanced protein-engineered polymers to fabricate fibers as building blocks for further bottom-up assembly according to the principles of textile engineering. The universality of the approach was confirmed by using a library of ELRs with different functionalities, followed by a "collect & click" strategy. Specifically, this encompasses i) the selection of ELRs with desired properties from the library and ii) the use of catalyst-free click chemistry to combine the chosen components. The so-formed elastin-like fibers featured customized porosity and were compatible with terminal sterilization schemes, maintaining their structural and biological integrity. Indeed, the fibers supported the attachment and alignment of human endothelial cells (ECs), and were further assembled in hierarchical patterns, resulting in a highly attractive and versatile platform that can be used to build up tissue equivalents.

2. Results and Discussion

2.1. Fabrication of Elastin-Like Fibers and Structural Characterization

We fabricated elastin-like fibers using a microinjection molding technique (**Figure 1**a,b). The approach enabled to fabricate fibers with lengths of more than 3 meters, and the diameter of the resulting fibers was easily controllable by changing the diameter of microinjection molding to 500 µm (ØS) and 1000 µm (ØL). Importantly, the production of the fibers did not require toxic reagents or cross-linkers thanks to the reactive groups in each ELR that enabled catalyst-free click chemistry.

We demonstrated the universality of our micro-fabrication approach by using three types of ELRs with varying functionalities. These included protease sensitive (DRIR) and structural (VKV) variants, which were coupled to ELRs containing the RGD sequence for enhanced bioactivity (Figure 1c and Table S1, Supporting Information).

Analysis of the fibers by confocal microscopy and scanning electron microscopy (SEM) revealed a homogeneous and smooth fiber surface, with sub-micrometer pores (**Figure 2**, first column, and Figure S1, Supporting Information).

To increase the versatility of our approach, we also implemented a salt-leaching gas-foaming (SL/GF) step during the micro-fabrication process, allowing us to tune the microstructure of the fibers by incorporating a porogen. Microscopic analysis confirmed the effectiveness of the approach in increasing the porosity when compared to the plain fibers in which no SL/GF was performed (Figure 2; Figure S2, Supporting Information). The fibers featured a uniform distribution of open pores both in cross sections and along their length, without any clustering, even in the fibers with a small diameter.

Quantitative analysis showed a good correlation between the size range of the sieved porogen particles (<40 µm and <100 µm) and the average pore size in the resulting fiber (Figure 2b). When the porogen size was <40 µm, the average pore size was 34 ± 5 µm for the ØS fibers and 42 ± 10 µm for the ØL fibers. When the porogen size was <100 µm, the average pore size increased to 89 ± 10 µm for ØS fibers and 108 ± 10 µm for ØL fibers. This highlights the ability to control the pore size of the fibers, irrespective of the fiber diameter. It is notable that we succeeded in fabricating fibers only 500 µm in diameter with pore diameters of ≈100 µm, creating thin and highly porous elastin-like fibers, the first of their kind. Previous studies showed the fabrication of tropoelastin-containing yarns composed of densely packed electrospun nanofibers.[34] Those approaches relied on blending the elastic material (tropoelastin) with a second material (e.g., silk fibroin, PCL), necessary to ensure structural integrity.[34,35] The

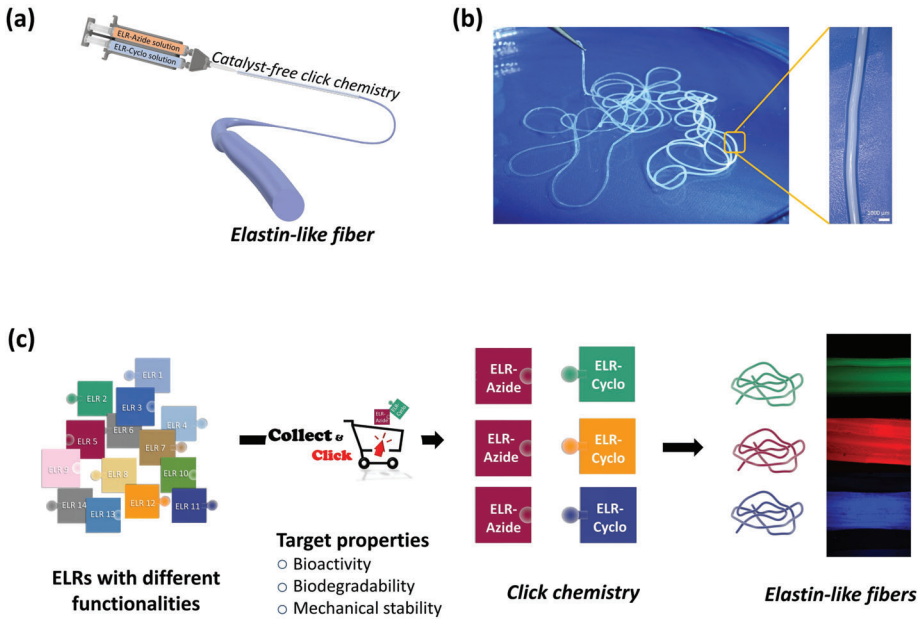

Figure 1. Fabrication of elastin-like fibers. a) Schematic of the fabrication of elastin-like fibers using the microinjection molding technique. b) Image (and close-up) of the resulting elastin-like fiber. c) Outflow of the "collect & click " strategy, which enables a high level of versatility in the molecular composition of the resulting fiber. This consists of first collecting the specific polymers from a library of elastin-like recombinamers (ELRs) with diverse functionalities, and then using click chemistry to fabricate the fibers. To visually demonstrate this concept, we selected three different sets of ELRs from the library. Confocal visualization was enabled by either fiber autofluorescence (excitation wavelength 405 nm, blue fiber) or functionalization of the ELRs with fluorescent labels. Specifically, N-hydroxysuccinimide (NHS)-ester fluorescein (excitation wavelength 488 nm) was used for one set of ELRs (green fiber) and Cyanine5.5 NHS ester (excitation wavelength 561 nm) for another (red fiber).

lack of a crosslinking method to stabilize the tropoelastin within the composite yarn also resulted in its partial loss.[35] Our fiber fabrication process offers a practical approach that capitalizes on the benefits of catalyst-free click chemistry to obtain pure elastin-like fibers with customized porosities, with no need for blending materials. The average pore sizes in our study ranged from 34 µm to 108 µm, providing ample space for cell infiltration, nutrient diffusion, and tissue ingrowth.[36–38] We also fabricated macroporous fibers using an alternative ELR combination based on structural DRIR-ELR and bioactive RGD-ELR (Figure S2, Supporting Information). This demonstrates the versatility of the applied strategy, which is not limited to a specific ELR and can be applied to ELRs with different functionalities, tailorable *ad-hoc* by recombinant methods. Overall, this method allows an unparalleled degree of customization, facilitating the production of fibers varying in molecular composition, length, diameter, and pore size.

2.2. Mechanical Characterization

The mechanical properties of the elastin-like fibers were systematically investigated by tensile testing (**Figure 3**). The stress–strain curves revealed an excellent stretching performance, with an elongation at break that reached 498 ± 45% of strain for the plain fibers (Figure 3), thereby indicating their ability to be stretched nearly six times their initial length. This was corroborated by manual stretching up to 500% of the initial fiber length (Figure 3a). The porous fiber showed less but still remarkable elongation of 173 ± 11% of strain, which could be attributed to the presence of pores acting as stress concentrators, potentially leading to the premature failure of the material.[39]

The mechanical performance of the fibers was extensively evaluated by cyclic testing. Specifically, the fibers were subjected to 10 cycles of loading and unloading, with plain fibers stretched to 200% and porous fibers to 60% of their initial length, followed by stretching to break. Notably, no hysteresis loop was observed between the loading and unloading cycles for the plain or porous fibers (Figure 3b). The elastin-like fibers returned to their original shape after deformation, making them suitable for applications that require repetitive loading and unloading (e.g., cardiovascular applications). This matches the intrinsic behavior of natural elastin, which undergoes high deformation without rupture and returns to its original state once the stress is removed.[40]

The Young's modulus (the slope of the initial part of the stress–strain curve) of the plain fibers (26 ± 10 kPa) was significantly higher than that of the porous fiber (17 ± 4 kPa). The maximum slope (maximum tangent modulus) of their stress–strain curves differed significantly, with values of 130 ± 69 kPa for the plain fibers and 36 ± 5 kPa for the porous fibers. The plain fibers were therefore much stiffer than the porous ones, particularly at the highest levels of strain. Additionally, the ultimate tensile strength of the plain fibers was 231 ± 101 kPa, whereas that of the porous fibers was 46 ± 6 kPa.

This comparison of mechanical properties provides valuable insights into the influence of porosity on the performance of elastin-like fibers. This will facilitate the design and optimization of ELR-based materials, offering new possibilities for tailoring

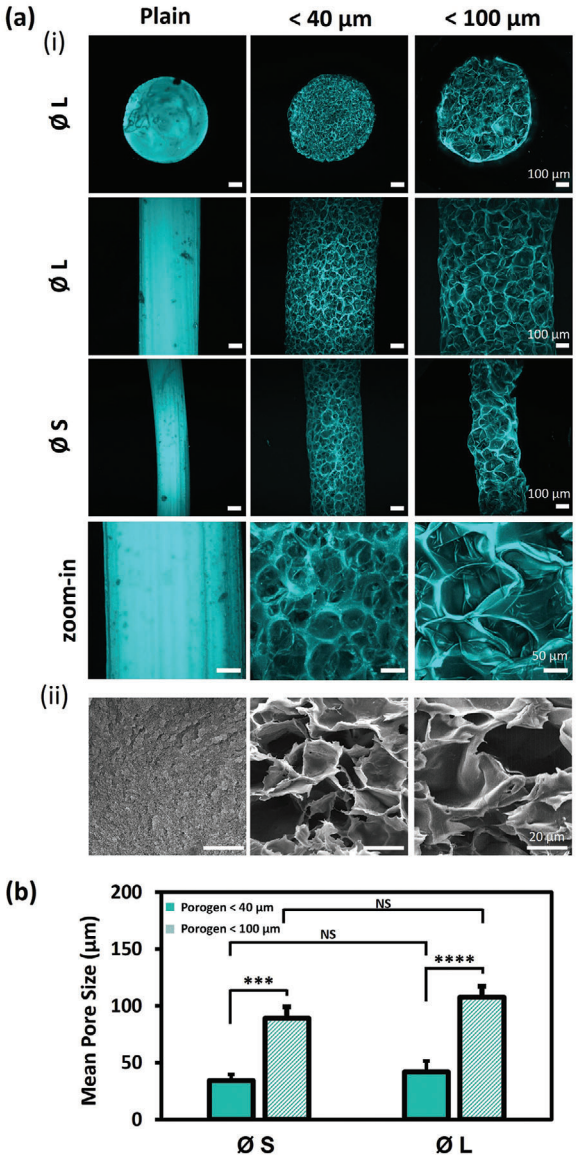

Figure 2. Microstructural characterization of elastin-like fibers prepared from ELR-VKV and ELR-RGD. a) Visualization of the microstructure by i) confocal microscopy and ii) SEM. The first column shows plain fibers whereas the second and third columns show the microstructure obtained by implementing a SL/GF step during the fabrication process (ØL and ØS refer to fibers fabricated using a microinjection tube of 1000 and 500 µm, respectively). b) Quantitative analysis of the pore sizes. Data are means ± SD (n ≥ 3). Statistical significance was determined by two-way ANOVA with Holm-Šidák comparison (*$p < 0.05$, **$p < 0.01$, ***$p < 0.001$, ****$p < 0.0001$; NS = nonsignificant).

the mechanical properties of these fibers to suit specific requirements.

2.3. Effect of Terminal Sterilization on the Material Properties

For any implant to advance toward clinical use, it is necessary to test and validate aspects such as sterilization. Here, we explored whether sterilization processes (ethanol treatment and autoclaving) had an impact on the mechanical and structural properties of the elastin-like fibers. Microscopic visualization of the porous fibers revealed no structural change (e.g., no collapsing of pores) after either of the sterilization treatments (**Figure** 4a; Figures S3 and S4, Supporting Information). This finding was supported by the quantitative analysis of porosity (Figure 4b). We observed comparable average pore sizes for non-treated (34 ± 1 µm), ethanol treated (37 ± 2 µm), and autoclaved (39 ± 5 µm) elastin-like fibers prepared using the <40 µm porogen ($p > 0.5$). We also observed comparable average pore sizes for non-treated (105 ± 14 µm), ethanol treated (115 ± 29 µm), and autoclaved (103 ± 8 µm) elastin-like fibers prepared using the <100 µm porogen ($p > 0.5$).

The thermal resistance exhibited by these materials is probably a consequence of their intrinsically disordered nature, enabling the ELRs to respond to and accommodate changes in temperature in a reversible manner. To confirm this hypothesis, we analyzed the ELRs by circular dichroism (CD) spectroscopy before and after autoclaving (Figure S6, Supporting Information). The ELR conformational state is temperature dependent due to their lower critical solution temperature (LCST) phase behavior.[41] Accordingly, the CD spectra were recorded at different temperatures (5, 37 and 60 °C) in order to determine whether the LCST behaviour persisted after autoclaving (Figure S6, Supporting Information). Typically, protein polymers derived from elastin exhibit a negative band at ≈197 nm (indicative of random coils) and a positive shoulder or peak at ≈210 nm (correlated to type II β-turns), and the amplitude of those bands is temperature-dependent.[42] The CD spectra for the ELRs at 5 °C included a positive shoulder at 210 nm and a prominent negative peak ≈197 nm, which indicates a predominantly disordered structure.[42] By increasing the temperature to 37 °C, the signal at 197 nm became weaker, whereas the magnitude of the peak at 210 nm increased, thus indicating an increase of type II β-turns.[43,44] When increasing the temperature to higher values (60 °C), the peak at 210 remained, while the amplitude of the band at 197 nm further decreased, indicating a concomitant decreased in disordered structures.[44] The reversible conformational changes correlated with the reversible thermo-responsive behavior of the ELRs (Figure S6, Supporting Information).

The mechanical characterization of the porous fibers before and after sterilization indicated no notable changes in the Young's modulus, ultimate tensile strength, elongation, and maximum tangent modulus (Figure 4d; Figure S5, Supporting Information). This was further evidenced by the overlap of the strain-stress curves (Figure 4c ii). The porous fibers therefore maintained their mechanical properties and integrity even after sterilization by ethanol treatment or autoclaving. For the plain elastin-like fibers, no significant change was observed in the mechanical properties after ethanol treatment, with the exception of a decrease in the Young's modulus, from 21 ± 3 kPa in untreated plain fibers to 13 ± 5 kPa in those treated with ethanol ($p = 0.01$). In contrast, autoclaving the plain fibers resulted in a significant increase in the mechanical properties, as evidenced by the increased slope on the strain-strain curve when compared to non-treated and ethanol treated fibers (Figure 4c i). The Young's modulus, which was 21 ± 3 kPa for untreated fibers, increased to 58 ± 6 kPa for autoclaved fibers ($p < 0.0001$). Similarly, the

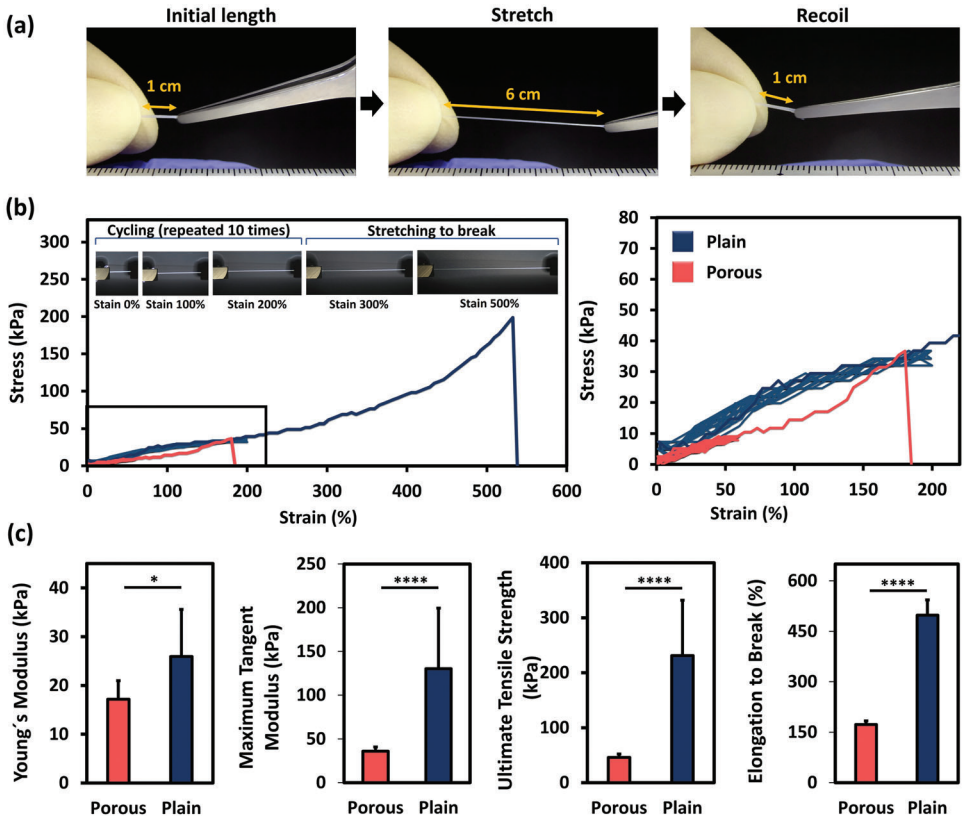

Figure 3. Mechanical characterization of elastin-like fibers prepared from ELR-DRIR and ELR-RGD. a) Captured video frames depicting the initial length (left image), the fiber stretched manually to 500% of its original length (central image), and the recoiled fiber that has returned to its original state once the stress is removed (right image). b) Representative stress–strain curves of the macroporous and plain elastin-like fibers, undergoing 10 cycles of loading and unloading followed by stretching to break. The graph on the right represents a close-up view of the stress–strain curves c) Young's moduli, maximum tangent moduli, ultimate tensile strength, and elongation at break for the macroporous and plain elastin-like fibers. Data are means ± SD ($n \geq 3$). Statistical significance was determined using a t-test (*$p < 0.05$, **$p < 0.01$, ***$p < 0.001$, ****$p < 0.0001$).

maximum tangent modulus increased from 98 ± 31 kPa to a remarkable 242 ± 125 kPa ($p < 0.0001$). The ultimate tensile strength also increased significantly from 193 ± 42 kPa to 431 ± 197 kPa ($p < 0.0001$). Remarkably, the elongation at break was not compromised by terminal sterilization (autoclaving) because there was no significant difference between the non-treated elastin-like fibers and of those subjected to autoclaving. The autoclaved fibers continued to exhibit an outstanding elongation of 447 ± 96%. Overall, the fibers maintained their structural integrity and no detrimental effect on the mechanical properties was observed, suggesting that the peptide bond remains largely unaffected. This was further supported by FTIR-ATR spectra of non-autoclaved and autoclaved elastin-like fibers, that showed the same patterns in all the bands associated with the amide group of the peptide bond (Figure S7, Supporting Information).[45]

In order to guarantee the safety and efficacy of fibers for clinical purposes, it is necessary to determine the most suitable sterilization approach at an early stage of development.[46] Although ethanol treatment is a commonly used disinfectant approach in vitro, it should not be deemed as a sterilization method. Radiation is one of the most commonly used methods for the sterilization of protein-based scaffolds. However, radiation of water-containing systems (e.g., hydrogels) can lead to radical formation due to water radiolysis, with the concomitant detrimental effects.[47] In the context of clinical implementation, terminal sterilization by autoclaving[48] is the preferred method, as recommended by the European Medicines Agency,[49] and it is particularly advantageous due to its reliability, absence of toxicity, and lack of residual chemicals or by-products. However, the ability of biomaterials to maintain their structural, chemical and biological integrity during the sterilization process is a major challenge.[48] Specifically, protein-based materials (including those forming the native ECM and bioinspired counterparts) are intrinsically prone to denaturation, in which external stress (such as heat) causes them to lose their native quaternary, tertiary and/or secondary structure. Any alterations or degradation caused by autoclaving can negatively affect the overall performance and functionality of the scaffolds. This has led many authors to generalize that autoclaving and biobased materials are incompatible[48,50,51] because thermal treatment (121°C) would lead to detrimental effects related to their mechanical properties, bioactivity and/or structure.

The ELRs are derived from peptide sequences found in the intrinsically disordered domains of natural elastin. Therefore, their properties do not reside in specific secondary or tertiary structures prone to denaturation. Our findings show that the elastin-like fibers can indeed be autoclaved, with either no effect on their mechanical performance (macroporous fibers) or an

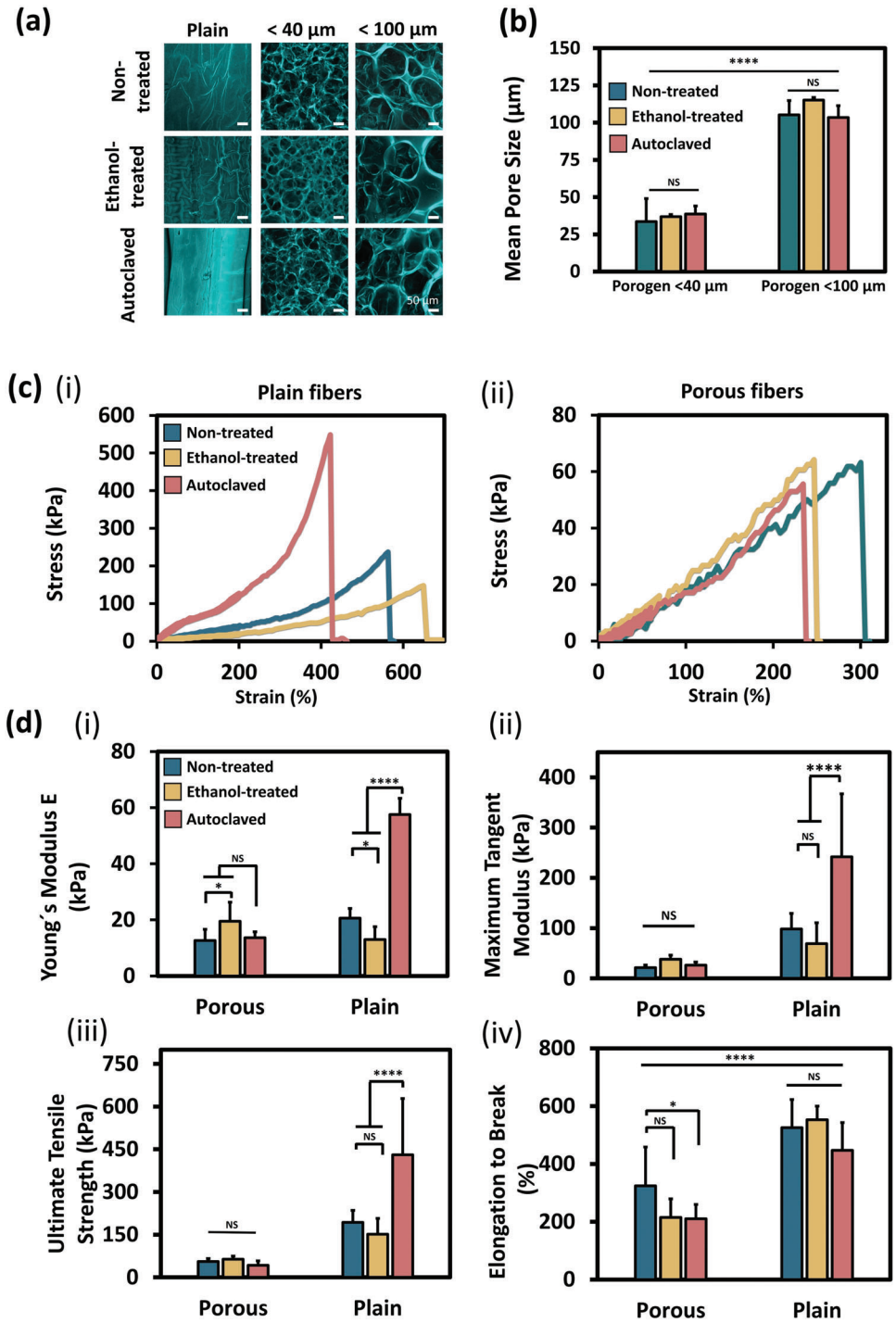

Figure 4. Impact of sterilization on the material properties of elastin-like fibers prepared from ELR-DRIR and ELR-RGD. a) Confocal images showing the microstructure of plain and macroporous fibers following different sterilization techniques. The images were taking by capturing the inherent autofluorescence of the ELRs. b) Quantification of the pore size of the fibers following different sterilization treatments. c) Representative stress–strain curves of the i) plain and ii) macroporous elastin-like fibers exposed to different sterilization techniques. The fibers were subjected to 10 cycles of loading and unloading followed by stretching to break. d) Evaluation of Young's moduli, maximum tangent moduli, ultimate tensile strength, and elongation at break for plain and macroporous elastin-like fibers treated with different sterilization methods. Data are means ± SD ($n \geq 3$). Statistical significance was determined by two-way ANOVA with Holm-Šidák comparison (*$p < 0.05$, **$p < 0.01$, ***$p < 0.001$, ****$p < 0.0001$; NS = non-significant).

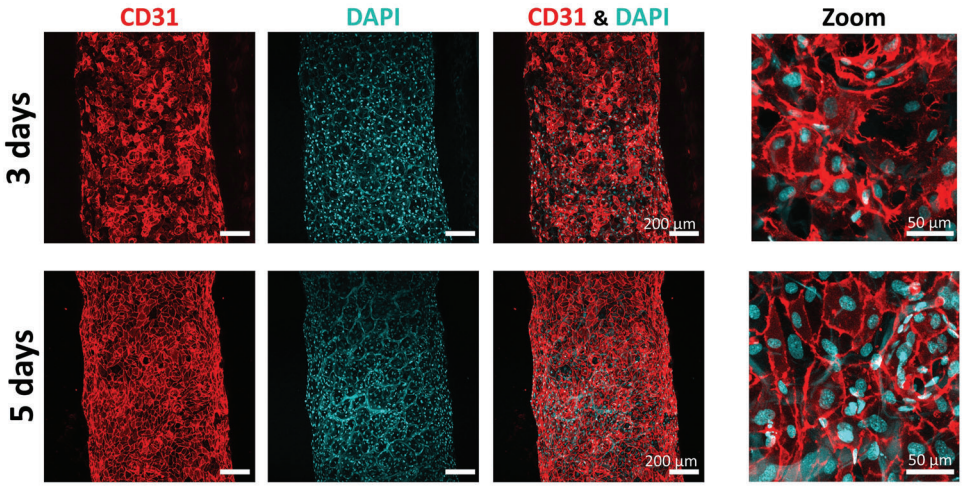

Figure 5. Confocal images of elastin-like fibers (prepared by mixing ELR-RGD and ELR-DRIR) cultured with primary human umbilical vein endothelial cells (HUVECs) for 3 and 5 days under static conditions. Endothelial cells are stained with antibodies against the CD31 marker (red) and counterstained with DAPI to reveal the nuclei (turquoise).

increase in stiffness, maximum tangent modulus, and ultimate tensile strength, while still maintaining the initial outstanding elasticity (plain fibers). This suggests that autoclaving may improve the mechanical performance of the plain fibers, making them potentially more suitable for certain applications where increased stiffness and strength are desired. Terminal sterilization by autoclaving did not compromise the ability of ELR molecules to accommodate, in a reversible manner, the typical conformational changes associated with thermo-responsive behavior (Figures S6, S8 and S9, Supporting Information). Thus, we hypothesize that the phenomena responsible for changes in the mechanical properties of the plain ELR fibers lies rather at the supramolecular level. Supramolecular interactions could be favored in the dense structure of the plain fibers, leading to further packing of the polymer chains. In the porous fiber, the open porosity would hinder tighter physical interactions due to the void spaces, explaining why the mechanical properties of the fibers before and after autoclaving are equivalent. The different impact of autoclaving plain and porous fibers shows how the suitability of a sterilization approach should be evaluated in the context of the final construct, rather than the bulk material, and at an early stage of implant development. Here, we demonstrate for the first time that engineered elastin can be autoclaved, which provides additional opportunities for the application of these protein-engineered polymers.

2.4. Biological Characterization

The fibers subjected to terminal sterilization (autoclaved) were seeded with primary human umbilical vein endothelial cells (HUVECs). A continuous and homogeneous layer with well-formed cell-to-cell junctions was observed within just 5 days, as revealed by confocal images of CD31-stained samples counterstained with DAPI (**Figure 5**). At this stage, the ECs exhibited an elongated and flattened morphology, with no specific orientation. Moreover, autoclaving did not compromise the ability of elastin-like fibers to support EC adhesion (Figure S10, Supporting Information) or proliferation (Figure S11, Supporting Information). The cellular performance also speaks for the absence of toxic compounds (e.g., ethanol), as also demonstrated by gas chromatography-mass spectrometry (Figure S12, Supporting Information).

The ability of elastin-like fibers to support EC attachment is highly relevant in TE, particularly for cardiovascular applications, because these cells play major roles in the regulation of vascular tone, inflammation, blood clotting, and angiogenesis.[52] However, proper tissue morphogenesis, homeostasis, and functional regeneration require not only cellular attachment, but also coordinated cellular alignment.[53] This is triggered by mechanical cues such as shear stress from the blood flow and cyclical stretch due to dilation across the vessel wall caused by the pulsatile nature of the blood flow.[54]

The elastin-like fibers cultured with HUVECs were exposed to uniaxial cyclic stretching, selected to mimic the physiological values reported in human arteries.[55,56] The stretching therefore ranged from 5% to 10% at a frequency of 0.5 Hz for a total of 24 h (**Figure 6a**).[57] We observed a clear reorientation of cells, which was largely dependent on the deformation magnitude. At stretching magnitudes of 5% and 8%, the cells continued to adapt to the topography of the fibers by assuming the shape of the pores, with a relatively chaotic organization of cytoskeletal actin filaments (Figure 6b). However, the cells began to align when the stretching magnitude reached 10%. This was confirmed by the arrangement of the actin filaments, which adopted a near parallel disposition.

The orientation of cells was quantified on the plain and porous fibers (Figure 6c). In both cases, cell elongation was followed by a collective change in cell alignment. The orientation of cells was more prominent in the plain fibers, suggesting that the macroporosity of the porous fibers hinders cell elongation and acts as a geometrical constraint on cell orientation. This highlights the significance of topographical cues in directing cell behavior.[58–60] Remarkably, the cells exhibited a strong tendency

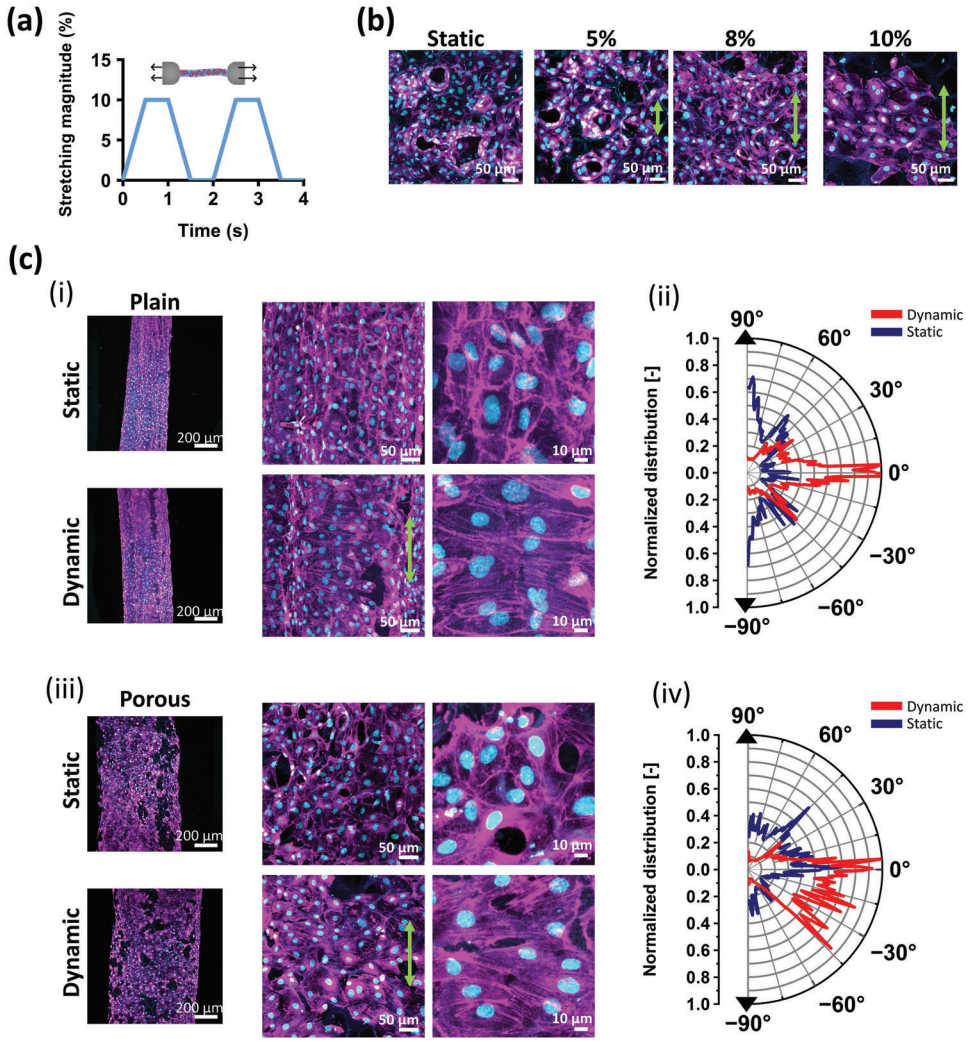

Figure 6. Cultivation of HUVECs on elastin-like fibers (ELR-RGD and ELR-DRIR) followed by mechanical stimulation. a) Diagram of the cyclic strain waveform used in the study. b) Confocal images of HUVEC-seeded elastin-like fibers subjected to various stretching magnitudes (0%, 5%, 8% and 10%). The green arrow indicates the axis of the stretching. c) Analysis of fibers. i) Confocal images of plain fibers seeded with HUVECs under static and dynamic (10% stretching) conditions. ii) Quantification of cellular alignment in the plain fibers (the direction of the stretching is represented by the black arrow). iii) Confocal images of macroporous fibers seeded with HUVECs under static and dynamic conditions (10% stretching). iv) Quantification of cellular alignment in the porous fibers. Phalloidin staining (violet) and DAPI (turquoise) were used to visualize the actin cytoskeleton and nuclei, respectively.

to align perpendicular to the direction of the stretch, which is consistent with the response of ECs to cyclic stretching as reported in the literature.[61,62] In the vessel wall, strain is circumferential, and the tendency of ECs to reorient perpendicular to the applied cyclic strain leads to EC alignment in the axial direction of the vascular wall.[63] Elastin-like fibers provide a soft microenvironment that closely mimics that of the ECM, making them a powerful platform for the analysis of cellular behavior in physiological environments.

2.5. Feasibility of the Bottom-Up Approach

The bottom-up assembly of biobased fibers is a promising approach for the construction of complex tissues and organs. We tested the feasibility of using the elastin-like fibers to fabricate hierarchically organized 2D and 3D structures by knitting, winding, weaving, and braiding. Both the plain and porous elastin-like fibers displayed an exceptional ability to bend without kinking (**Figure** 7a,i and iii) and to be tied off by knotting (Figure 7a,ii,iv). Knot-based assembly techniques like knitting can be used to create 3D geometries, as currently implemented in the medical implant industry.[64] Indeed, we used the weft knitting technique to produce a knitted scaffold that is highly elastic and stretchable (Figure 7b,ii and Video S1, Supporting Information).

We successfully collected fibers of multimeter length onto a bobbin without compromising the diameter or length of the fibers (Figure 7b). The elastin-like fibers were also assembled into woven (Figure 7b,v) and braided structures (Figure 7) that

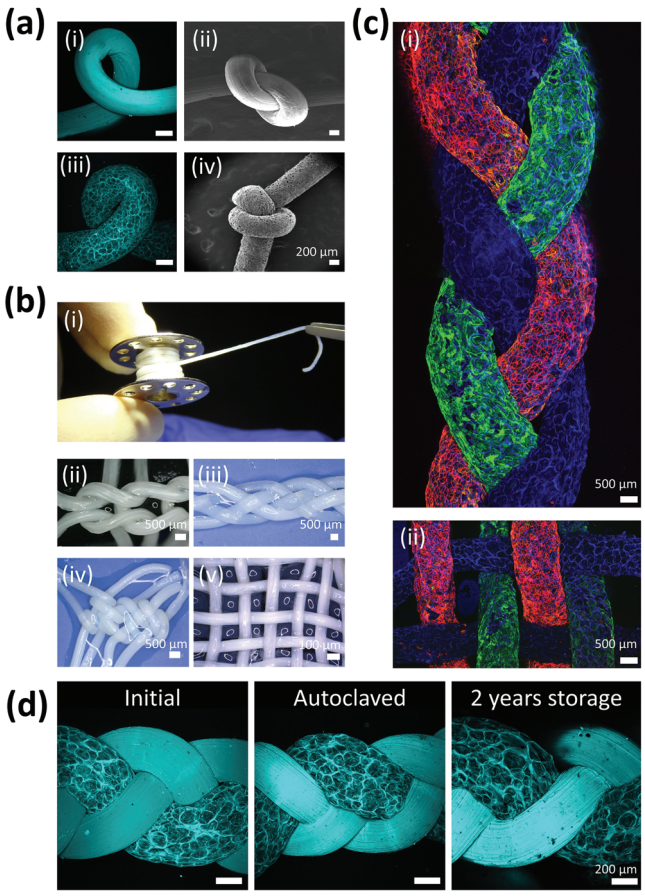

Figure 7. Feasibility of the bottom-up approach. a) Confocal and scanning electron microscopy (SEM) images showing the flexibility of the elastin-like fibers through bending and knotting, i,ii) plain fiber and iii,iv) porous fiber. b) Image of i) a multi-meter elastin-like fiber coiled on a bobbin, as well as ii) knitted, iii) braided, iv) soumak woven, and v) tabby woven elastin-like fibers. c) Elastin-like fibers cultured with human umbilical vein endothelial cells (HUVECs) and organized into textile patterns such as braiding and weaving. To facilitate the distinction of each fiber along the braided or knitted structure, each fiber was differentially stained with either an anti-CD31 antibody (red) to detect endothelial cells, or phalloidin (green) to detect the actin cytoskeleton. The blue fibers were unstained, and visualized thanks to their autofluorescence. d) Confocal images of a hybrid braided structure composed of two plain fibers and one porous fiber. The structure was autoclaved, stored for 2 years at room temperature in a solution of 70% ethanol and washed in PBS before imaging.

were easy to manipulate. To further demonstrate the potential of this approach, we created a hybrid braided structure composed of plain and porous fibers. Confocal images of the resulting structure confirmed the successful interlocking of the porous and plain fibers (Figure 7d). To exploit the thermal resistance of these materials, we autoclaved and successfully stored the braided fibers for 2 years (Figure 7d). This confirms such textile constructs have the potential to be offered as off-the-shelf products, a preferred option in the biomedical field that promotes clinical adoption and allows the use of such products in emergency cases.[65,66]

One significant advantage of the textile approach is its potential to automate tissue fabrication.[5] To advance in that direction, we developed a custom-made circular loom, reducing the manual handling of the fibers and allowing us to fabricate a homogenous weaved tubular textile (**Figure 8**). To the best of our knowledge, this is the first ever tubular textile made solely from engineered elastin. Notably, fiber-like hydrogels tend to lack mechanical strength and are difficult to handle, making conventional methods for creating textile constructs challenging when using such materials.[7] However, the elastin-like fibers were robust enough to overcome these obstacles, allowing their use for textile-like assembly.

Such tubular constructs could facilitate the realization of vascular prosthesis in the future. Vascular tissue engineering is not yet a routine clinical approach, despite the clear medical need and market demand. For example, the L'Heureux group developed vascular prosthesis derived from sheets of cell-assembled ECM that were rolled into tubes, matured in vitro, endothelialized and implanted into patients.[67] However, the method was too complex and laborious for the economic preparation of grafts. More recently, the same group introduced textile technologies during the manufacturing scheme, which allows more versatility, and a faster and automatable production.[68] Even so, the yarn is still based on devitalized tissue, and requires a complex in vitro cell culture phase. The Niklason laboratory pioneered grafts based on decellularized ECM generated in vitro[69,70] These constructs decouple the in vitro culture and implantation phases, focusing on the use of allogenic rather than autologous cells. Accordingly, the manufacturing steps (cell isolation and expansion, tissue growth, and shipping) are carried out off-line, and the resulting grafts can be made available to patients needing rapid intervention. Phase 3 clinical trials are underway testing this concept as a means to facilitate vascular access for hemodialysis. However, these approaches still rely on tissue harvesting and/or cell isolation, with potential concomitant issues associated with unpredictable cell behavior during the production phase.

Alternative designs for tissue-engineered vascular prosthesis do not involve cells at any stage of production ("culture free") and do not rely on any donor material ("tissue free").[71] These approaches are more material-centric,[72] thus benefiting from potentially simpler adoption pathways. Their potential has been exemplified by the progress of some of these concepts to clinical trials.[73] However, these approaches has been thus far mainly focused on top-down fabrication processes such as electrospinning,[74] and the field could benefit from strategies that better recapitulate the complex hierarchical structure of native tissues.

Despite remarkable achievements in the field, TE vascular prosthesis continue to struggle to achieve commercial success. This indicates the need for disruptive innovations that can leap over the valley of death in a true bench-to-bedside approach.[75] Upcoming innovations should consider the pioneering work done so far in TE vascular grafts, and should implement lessons learnt into the design process. This includes a balance between graft functionality and economic feasibility, which is essential for successful translation.[76]

The technology presented herein is built on the principles of versatility, controllability, reproducibility and storage, enabling for the first time the production of tubular elastin-like textiles. We are still far from the pioneered concepts of vascular

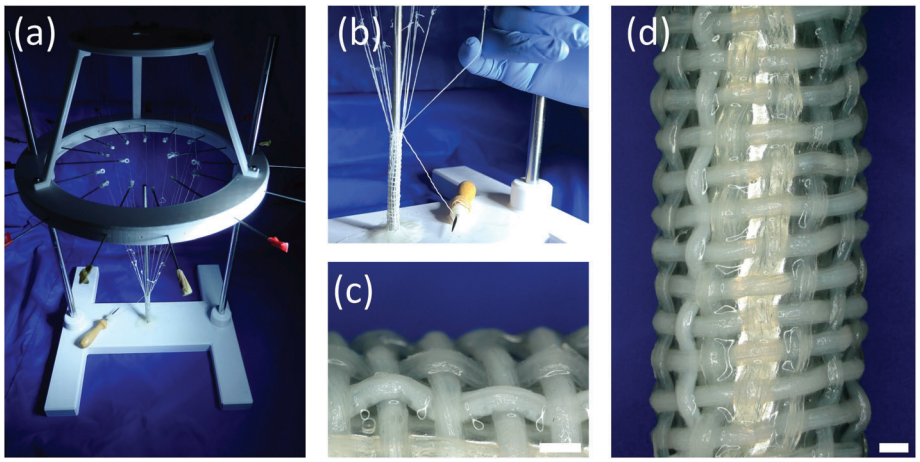

Figure 8. Textile-based assembly of elastin-like fibers (ELR-RGD and ELR-VKV) into tubular structures. a) Custom-made weaving loom, in which 15 longitudinal elastin-like fibers (15 cm) and one circumferential elastin-like fiber thread (2 m) are assembled. b) Detailed view of the fibers during the weaving process. c,d) Resulting woven tubular textile constructed from elastin-like hydrogel fibers. Scale bars = 1 mm.

prosthesis described above, but our technology provides the foundation for further exploration.

Textile-based assembly enables a further level of adaptability because the scaffold properties can be modulated not only by the inherent properties of the material but also by the hierarchical structure.[4,34] This expands the range of properties that can be achieved, and allows local and directional fine tuning in accordance with the intended application. For instance, the warp and the weft of the construct can be prepared from ELRs with different properties, including degradation rate. By incorporating different types of fibers in both the warp and weft, precise control over the mechanical properties can be achieved.[77] Overall, our approach integrates the customization and controllability provided by recombinant materials such as ELRs with the versatile assembly achieved using textile technologies. The new platform is not limited to high-value products in the biomedical field, but could also influence the garment industry, especially the development of long-lasting stretch fabrics. The ELR is a safe, renewable, non-animal product. This can pave the way for the manufacturing of clothes that could revolutionize the fabric industry. We have already witnessed examples in the past of material platform technologies that are applied both in the biomedical field and in the manufacture of everyday items. For instance, GORE-TEX is used both for the fabrication of high-value products like vascular grafts, and also as a breathable, waterproof fabric.

3. Conclusions

The platform presented herein offers precise control over the scaffold at multiple levels, ranging from the molecular level (polymers) to the micro (fibers) and macro (textile) levels. At the molecular level, we achieve this control through the custom-engineered design of the ELR chains. These ELRs serve as starting materials, which are then processed into microfibers with a precisely controlled microstructure. These microfibers are subsequently assembled into textiles. The toolbox that this platform embodies opens up exciting new possibilities for the development of medical implants, where strict reproducibility and standardized production are essential prerequisites.

4. Experimental Section

Design and Functionalization of the ELRs: The ELRs used in this study were VKV, RGD and DRIR, each selected for their specific properties. VKV is a structural recombinamer lacking bioactive sequences, whereas RGD contains a tripeptide (Arg-Gly-Asp) that promotes cell attachment and DRIR includes the cleavage site for urokinase plasminogen activator (Asp-Arg-Ile-Arg).[27,28] The recombinamers were chemically modified to carry azide and cyclooctyne groups by transformation of the ϵ-amine group present in the lateral chain of the lysine residue, as previously reported by us.[78] Briefly, for the functionalization of ELRs with cyclooctyne or azide groups, (1R,8S,9S)-bicyclo[6.1.0]non-4-yn-9-ylmethyl succinimidyl carbonate (SynAffix BV) or 2-azidoethyl (2,5-dioxopyrrolidin-1-yl) carbonate (GalChimia), respectively, were added to a 20 mg mL^{-1} ELR solution in anhydrous DMF under N_2 atmosphere. The resulting mixture was stirred at room temperature for 60 h. Afterwards, diethyl ether was added at a volume ratio 3:1, resulting in a white precipitate. The supernatant was discarded, and the white precipitate was washed three times in acetone. The so-obtained product was dried under vacuum pressure and afterwards resuspended in ultrapure water overnight (4 °C) and dialyzed against 25 L of ultrapure water at 4 °C (4 changes). The final product was lyophilized and stored at −20 °C until further use. The purity and monodispersity are systematically characterized by H-NMR and MALDI-ToF, respectively. Specifically, DRIR and VKV were modified to bear the cyclooctyne group, whereas RGD was modified to include the azide group. The detailed characteristics of the ELRs can be found in Table S1 (Supporting Information).

Fabrication of the Elastin-Like Fibers: The ELRs were dissolved in a 1:1 (v/v) mixture of phosphate-buffered saline (PBS; Thermo Fisher Scientific, USA) and ethanol (Sigma-Aldrich, USA) at room temperature to a final concentration of 100 mg mL^{-1}, as previously reported by us.[22,30–32] Two solutions containing ELRs modified with cyclooctyne and azide groups, respectively, were loaded into separate syringes and placed into a dual injector holder (Tisseel, USA). The solutions were co-extruded through a mixing nozzle (DMG, Germany) into a silicon tube (Cole-Parmer, USA) and were left for 20 min to crosslink. The resulting fiber was ejected and washed with PBS. The diameter and length of the fiber were controlled by adjusting the size of the silicon tube. To introduce macroporosity, a SL/GF strategy was used.[22] Specifically, $NaHCO_3$ particles were sieved to obtain two different size ranges (<40 µm and <100 µm) and dispersed in each

ELR solution at a weight ratio of 1:10 (recombinamer/particles). The solutions were co-extruded as described above, but the crosslinking reaction was extended to 30 min. The resulting elastin-like fibers were ejected and placed in 3 M citric acid for 30 min to dissolve the $NaHCO_3$ particles. The porous fibers were then washed three times with PBS for 16 h to eliminate any potential residues.

Sterilization of the Elastin-Like Fibers: Porous and plain ELR fibers were subjected to different sterilization schemes, and their effect on the microstructure and mechanical performance was systematically evaluated. For ethanol sterilization, the elastin-like fibers were immersed in 70% (v/v) ethanol for a minimum of 2 h followed by three washes with PBS. Alternatively, the fibers were autoclaved at 121 °C and 200 kPa for 15 min (dx-serie, Systec, Germany).

Microstructure Characterization: For SEM, the samples were first rinsed in PBS and then fixed in 3% glutaraldehyde in Sorensen's buffer at room temperature for 1 h. After fixation, the samples were dehydrated by immersing them in a graded ethanol series (40% to 100%, in 10% increments) for 15 min in each solution, followed by critical point drying in CO_2. The dried samples were then mounted on aluminum stubs and sputter coated with a 20-nm layer of gold-palladium. Images were captured using The Quattro S microscope (Thermo Fisher Scientific) with an accelerating voltage of 10 kV.

For brightfield imaging, samples were fixed in Carnoy's solution before embedding in paraffin, and were cut in 3-µm cross-sections, which were viewed using an AxioObserver Z1 epifluorescence microscope (Carl Zeiss, Germany). Images were acquired using an AxioCam MRm digital camera (Carl Zeiss) and analyzed with ImageJ software to quantify the porosity of the fibers. Three independent fibers were measured in three different regions per experimental condition.

For confocal microscopy, the samples were viewed using an inverted Zeiss LSM710 laser scanning confocal microscope fitted with an EC Plan-Neofluar 10× objective . The images were acquired sequentially by unidirectional line scanning using Zen Black 2012 software (Carl Zeiss). The elastin-like fibers were imaged by exploiting their autofluorescence when excited at 405 nm, with emission in the range 410–495 nm.

Mechanical Characterization: The mechanical characterization of the fibers was carried out using a UNIVERT tensile test instrument (CellScale, Canada) equipped with a 1-N load cell. To assess the stress applied to the fibers, the diameter of each fiber was measured using a digital microscope (Keyence, Japan). These measurements were taken at a minimum of five points along the fiber and the average diameter was used to calculate the cross section of the fiber before testing. The individual fibers within each sample type had a consistent diameter but there were minor differences between sample types (e.g., plain versus porous).

The fibers were immersed in a PBS bath heated to 37 °C and were clamped to the grips of the tensile test instrument 3–5 cm apart. To settle the % of stretching during the cycling testing, a preliminary test was done, in which the fibers were stretched until breakage, and 40% of the elongation at break for each type of fiber was selected as strain for the cyclic testing. For the systematic testing, the fibers were first subjected to 10 cycles of stretching from 0% to 200% strain, (for plain fibers) or from 0% to 60% strain (for porous fibers) using a constant strain rate of 0.15 mm s^{-1} . The fibers were then stretched to failure with the same constant strain rate. A stress-strain curve was plotted, and the initial elastic modulus (Young's modulus) and maximum tangent modulus were determined. The initial elastic modulus was calculated within the strain range of 0%–100% for the plain fibers and 0–50% for the porous fibers. The maximum tangent modulus was determined from the steepest slope, which depended on the experimental conditions. The ultimate tensile strength and the elongation to break were extracted from the stress-strain curve. The ultimate tensile strength was defined as the maximum stress reached by each sample during the test.

CD Spectroscopy: The ELRs were dissolved at a concentration of 1 mg mL^{-1} in ultrapure water. A 1:10 dilution was prepared immediately prior to each measurement, and was transferred to a quartz cuvette with a path length of 0.2 cm. The CD spectra were acquired using a Jasco J-815 150-S spectrometer, scanning over the wavelength range 190–260 nm. Points were acquired every 0.5 nm using a scan speed of 50 nm min^{-1}. Measurements were taken at temperatures of 5, 37 and 60 °C, and the reversibility of the conformational changes was also checked by recording after cooling (37 and 5 °C). Samples were equilibrated for 15 min before each measurement during heating, and for 30 min during cooling. Spectra were corrected by subtracting the corresponding blank solvent readings.

FTIR-ATR: Autoclaved and non-autoclaved elastin-like fibers (both fabricated by mixing ELR-RGD and ELR-VKV) were freeze-dried (Labconco lyophilizer) and evaluated by Fourier Transform Infrared Spectroscopy with Attenuated Total Reflectance (FTIR-ATR) in an infrared spectrometer (Tensor 27, Bucker). FTIR-ATR spectra were obtained with 128 scans per spectrum at a spectral resolution of 2 cm^{-1} in the wavenumber from 4000 to 600 cm^{-1}.

Differential Scanning Calorimetry (DSC): Elastin-like scaffolds were prepared by mixing ELR-RGD and ELR-VKV at a concentration of 100 mg mL^{-1}, washed with PBS and autoclaved (when applicable) as described above. The samples were cut with a biopsy punch (Miltex) of 5 mm diameter, placed in a standard 40-µL aluminum crucible and hermetically sealed. The same volume of PBS was placed in the reference crucible. The DSC experiments were carried out in a Mettler Toledo 822e with a liquid nitrogen refrigerator by applying an isothermal stage (5 min at 0 °C) and a heating ramp (2 °C min^{-1} from 5 to 50 °C).

Gas Chromatography-Mass Spectrometry: To test whether ethanol traces could remain in the click hydrogel, the ELRs were dissolved in a 1:1 (v/v) mixture of phosphate-buffered saline (PBS; Thermo Fisher Scientific, USA) and ethanol (Sigma–Aldrich, USA) at room temperature to a final concentration of 100 mg mL^{-1}, as described above, and co-injected in a disc mold (volume 1 mL). The resulting click-elastin-like hydrogels were demolded and rinsed in PBS as follows: 1) 25 mL PBS, 30 min; 2) 25 mL PBS, 30 min; 3) 50 mL PBS, 30 min; 4) 50 mL PBS, 16 h. Ethanol content was then determined by headspace-solid phase microextraction (HS-SPME) coupled to gas chromatography-mass spectrometry (GC–MS) (7890A; Agilent Technologies). Briefly, the samples (1 mL) were placed in 20-mL headspace vials with silicon septa and incubated at 40 °C, 250 rpm for 15 min. Samples were analyzed with 50/30 µm Divinylbenzene/Carboxen/Polydimethylsiloxane (DVB/CAR/PDMS) fibers for 30 min at 40°C. After sampling, the fiber was immediately inserted into the injection port of the GC equipment. An HP-INNOWAX column (60 m, 0.250 mm, 0.5 µm) (J &W Scientific, Folsom, CA, USA) was used. Helium flow was 1.2 mL min^{-1} and the temperature was programmed as follows: 40 °C for 5 min, increased to 80 °C at 2.5°C min^{-1}, and then maintained at that temperature for 5 min. A calibration curve was created with serial dilutions of ethanol in PBS from which the ethanol content in the hydrogel samples was quantified.

Cellular Studies Using the Elastin-Like Fibers: The elastin-like fibers were sterilized by autoclaving as described above and were left to cool before seeding with HUVECs isolated from human umbilical cords as previously described.[79] Human umbilical cords were obtained after written informed consent at University Hospital Aachen, Aachen, Germany and were provided by the RWTH Aachen University Centralized Biomaterial Bank (cBMB), in compliance with its regulations, following RWTH Aachen University Medical Faculty Ethics Committee approval (cBMB project number 323). HUVECs were cultured in endothelial growth medium 2 (EGM2; PromoCell, Germany) supplemented with fetal calf serum, epidermal growth factor, basic fibroblast growth factor, insulin-like growth factor, vascular endothelial growth factor 165, ascorbic acid, heparin, and hydrocortisone. The cells were expanded under standard culture conditions in a humidified 5% CO_2 atmosphere at 37 °C. Primary cells in passages 1–3 were used for all the experiments. After the HUVECs reached 80%–90% confluency, they were trypsinized and resuspended in EGM2 medium to achieve the desired cell concentration. The elastin-like fibers were coaxially introduced into a silicon tube and clamped at one end. A cell suspension containing 1.5 mL of cells at a concentration of 0.7×10^6 cells mL^{-1} was then introduced into the silicon tube, and the other end was also clamped. The silicon tube was placed in a sterile environment and rotated along the longitudinal axis at 1 rpm on an RS-TR 05 roller mixer (Carl Roth) for 2 h to facilitate cell attachment to the fibers. The fibers were then removed from the remaining cell suspension and placed in fresh culture medium for static cell culture.

For the dynamic culture, fibers from a 48-h static pre-culture were mounted on the MechanoCulture T6 (CellScale, Canada) in a humidified 5% CO_2 atmosphere at 37 °C and were mechanically stimulated for 24 h, undergoing uniaxial stretching (10% cyclic ramp stretch at 0.5 Hz). The control groups remained in static culture for 3 days.

Cell Staining, Visualization and Analysis of Cell Orientation: The fibers seeded with cells were washed with PBS and fixed with 4% methanol-free paraformaldehyde (Carl Roth) for 60 min at room temperature, then washed again three times with PBS. The samples were blocked for 1 h at room temperature with 0.5% normal goat serum (Agilent DaKo, USA) in 0.1% Triton X-100 (Sigma-Aldrich) and then incubated with a mouse primary monoclonal anti-CD31 antibody (Sigma–Aldrich) at a dilution of 1:10 to label the ECs. After washing as above, the samples were incubated for 1 h at room temperature with a goat anti-mouse IgG H6L secondary antibody conjugated to Alexa Fluor 594 (Invitrogen, USA) at a dilution of 1:400. Both antibodies were diluted in 1% bovine serum albumin (BSA; Sigma–Aldrich) in PBS. To visualize actin filaments, the cells were permeabilized by incubation in 0.1% Triton-X 100 in PBS for 5 min, rinsed three rinses with PBS, and then stained with phalloidin-iFluor 488 conjugate (Cayman Chemicals, USA) at a dilution of 1:1000 in 1% BSA. The samples were then incubated for 90 min at room temperature, rinsed three times with PBS and incubated for 15 min with 1 µg mL^{-1} DAPI (Carl Roth) in PBS to stain the nuclei, followed by three washes with PBS.

Samples were visualized by confocal microscopy as described above with excitation at 405 nm and emission in the range 410–495 nm for DAPI, excitation at 488 nm and emission in the range 495–630 nm for phalloidin-iFluor 488, and excitation at 561 nm and emission in the range 585–733 nm for the CD31-specific Alexa Fluor 594 staining. To determine the orientation of cells from the static and dynamic cultures, confocal images of phalloidin staining were analyzed with ImageJ[80] using the OrientationJ Distribution function and the cubic spline algorithm with a Gaussian window of 2 pix. No cell accumulation or overlaps were added to the measurements.

Impact of Autoclaving on the Bioactivity of Elastin-Like scaffolds: Autoclaved and non-autoclaved scaffolds were prepared by mixing ELRs (ELR-RGD and ELR-VKV) at a concentration of 100 mg mL^{-1} as described above. The non-autoclaved scaffolds were produced under sterile conditions to avoid any post-treatment, and the autoclaved counterparts were sterilized as described before (121 °C, 15 min). Human umbilical vascular endothelial cells were seeded at a concentration of 0.7×10^6 cells mL^{-1} and statically cultured for 24 h under standard culture conditions in a humidified 5% CO_2 atmosphere at 37 °C. The scaffolds were stained with an anti-CD31 antibody, counterstained with DAPI, and then imaged using a confocal microscope (inverted Zeiss LSM710 laser scanning confocal microscope).

Cell Proliferation on Autoclaved Elastin-Like Scaffolds: Elastin-like scaffolds were fabricated by mixing ELR-RGD and ELR-DRIR at a concentration of 100 mg mL^{-1}, as previously described. The scaffolds were sterilized by autoclaving (121 °C, 15 min) and seeded with HUVECs at a concentration of 1.7×10^5 cells mL^{-1}, and cultured for 2 h, 24 h, 72 h and 5 days (humidified 5% CO_2 atmosphere at 37 °C). The media was changed every two days. The scaffolds were stained with an anti-CD31 antibody, counterstained with DAPI, and then imaged using a confocal microscope (inverted Zeiss LSM710 laser scanning confocal microscope). The single-cell nuclei were counted using CellProfiler Image Analyst software[81] to quantify the number of cells at each time point. The pipeline consisted of the IdentifyPrimaryObjects module with diameter restrictions of 7 pixels to 30 pixels and adaptive thresholding parameters. The object outlines were drawn on the original image and manually inspected. Object counts were exported to a spreadsheet. The experiment was performed with n = 3 technical replicates for each time point.

Textile-Based Assembly: To assess the ability of the elastin-like fibers to form a higher-order 3D assembly, they were wound onto a bobbin and arranged in textile patterns using the techniques of weaving, knitting, and braiding. For the tubular weaved structure, one circumferential elastin-like-fiber (weft) was inserted between a movable and a fixed set of tensioned elastin-like fibers (warp) to create the woven textile in tubular form.

Statistical Analysis: Statistical differences were assessed using a t-test or two-way analysis of variance (ANOVA) followed by the *post-hoc* Holm-Šidák method. All experiments were conducted at least in triplicate ($n \geq 3$). The results are presented as means ± standard deviations (SD). The threshold for statistical significance was $p < 0.05$ ($*p < 0.05$; $**p < 0.01$; $***p < 0.001$; $****p < 0.0001$). Any value of $p > 0.05$ was defined as non-significant (NS).

Supporting Information

Supporting Information is available from the Wiley Online Library or from the author.

Acknowledgements

This work was funded by the NanoMatFutur Program of the German Federal Ministry of Education and Research (BMBF, grant number 13XP5136). JCRC was grateful for funding from the Spanish Government (PID2019-110709RB-I00 and PID2022-137484OB-I00). The scanning electron microscope (Quattro S) was funded by the Deutsche Forschungsgemeinschaft (DFG, German Research Foundation-495328185). The authors acknowledge the support of Prof. Dr. Müller-Newen, Dr. Ernst and the Confocal Microscopy Facility, a Core Facility of the Interdisciplinary Center for Clinical Research (IZKF) Aachen within the Faculty of Medicine at RWTH Aachen University. The authors also acknowledge the Library of Science & Medical Illustrations (https://www.somersault1824.com).

Open access funding enabled and organized by Projekt DEAL.

Conflict of Interest

The authors declare no conflict of interest.

Data Availability Statement

The data that support the findings of this study are available from the corresponding author upon reasonable request.

Keywords

bottom-up, engineered elastin, fibers, hierarchy, textile

Received: October 24, 2023
Revised: January 29, 2024
Published online: February 10, 2024

[1] A. Levin, T. A. Hakala, L. Schnaider, G. J. L. Bernardes, E. Gazit, T. P. J. Knowles, *Nature Reviews Chemistry* **2020**, *4*, 615.
[2] N. Mittal, F. Ansari, K. Gowda V, C. Brouzet, P. Chen, P. T. Larsson, S. V. Roth, F. Lundell, L. Wågberg, N. A. Kotov, L. D. Söderberg, *ACS Nano* **2018**, *12*, 6378.
[3] A. D. Theocharis, S. S. Skandalis, C. Gialeli, N. K. Karamanos, *Adv. Drug Delivery Rev.* **2016**, *97*, 4.
[4] A. Tamayol, M. Akbari, N. Annabi, A. Paul, A. Khademhosseini, D. Juncker, *Biotechnol. Adv.* **2013**, *31*, 669.
[5] A. Doersam, O. Tsigkou, C. Jones, *Adv. Mater. Technol.* **2022**, *7*, 2101720.
[6] R. D. Pedde, B. Mirani, A. Navaei, T. Styan, S. Wong, M. Mehrali, A. Thakur, N. K. Mohtaram, A. Bayati, A. Dolatshahi-Pirouz, M. Nikkhah, S. M. Willerth, M. Akbari, *Adv. Mater.* **2017**, *29*, 1606061.

[7] M. Akbari, A. Tamayol, S. Bagherifard, L. Serex, P. Mostafalu, N. Faramarzi, M. H. Mohammadi, A. Khademhosseini, *Adv. Healthcare Mater.* **2016**, *5*, 751.
[8] Y. Jiao, C. Li, L. Liu, F. Wang, X. Liu, J. Mao, L. Wang, *Biomater. Sci.* **2020**, *8*, 3574.
[9] P. T. Phan, M. T. Thai, T. T. Hoang, J. Davies, C. C. Nguyen, H.-P. Phan, N. H. Lovell, T. N. Do, *Sci. Rep.* **2022**, *12*, 11067.
[10] C. Jiang, K. Wang, Y. Liu, C. Zhang, B. Wang, *Acta Biomater.* **2021**, *128*, 60.
[11] L. Miao, F. Wang, L. Wang, T. Zou, G. Brochu, R. Guidoin, *Materials* **2015**, *8*, 8148.
[12] D. Altman, T. Väyrynen, M. E. Engh, S. Axelsen, C. Falconer, *International Urogynecology Journal* **2008**, *19*, 787.
[13] F. A. Ganj, O. A. Ibeanu, A. Bedestani, T. E. Nolan, R. R. Chesson, *International Urogynecology Journal* **2009**, *20*, 919.
[14] C. Singh, C. S. Wong, X. Wang, *Journal of functional biomaterials* **2015**, *6*, 500.
[15] A. De Martino, A. D. Milano, G. Thiene, U. Bortolotti, *Ann. Thoracic Surge.* **2020**, *110*, 1427.
[16] M. Kun, C. Chan, S. Ramakrishna, A. Kulkarni, K. Vadodaria, in *Advanced Textiles for Wound Care*, (Second Edition), (Ed: S. Rajendran), Woodhead Publishing, Sawston, UK **2019**.
[17] M. S. B. Reddy, D. Ponnamma, R. Choudhary, K. K. Sadasivuni, *Polymers* **2021**, *13*, 1105.
[18] A. M. J. Coenen, K. V. Bernaerts, J. A. W. Harings, S. Jockenhoevel, S. Ghazanfari, *Acta Biomater.* **2018**, *79*, 60.
[19] A. Ibáñez-Fonseca, T. Flora, S. Acosta, J. C. Rodríguez-Cabello, *Matrix Biol.* **2019**, *84*, 111.
[20] D. Miranda-Nieves, E. L. Chaikof, *ACS Biomater. Sci. Eng.* **2017**, *3*, 694.
[21] S. Yi, F. Ding, L. Gong, X. Gu, *Curr. Stem Cell Res. Ther.* **2017**, *12*, 233.
[22] A. Fernández-Colino, F. Wolf, H. Keijdener, S. Rütten, T. Schmitz-Rode, S. Jockenhoevel, J. C. Rodríguez-Cabello, P. Mela, *Mater. Sci. Eng., C* **2018**, *88*, 140.
[23] A. Girotti, A. Fernández-Colino, I. M. López, J. C. Rodríguez-Cabello, F. J. Arias, *Biotechnol. J.* **2011**, *6*, 1174.
[24] A. Ibáñez-Fonseca, S. Santiago Maniega, D. Gorbenko del Blanco, B. Catalán Bernardos, A. Vega Castrillo, Á. J. Álvarez Barcia, M. Alonso, H. J. Aguado, J. C. Rodríguez-Cabello, *Frontiers in Bioengineering and Biotechnology* **2020**, *8*.
[25] G. Marsico, C. Jin, S. A. Abbah, E. M. Brauchle, D. Thomas, A. L. Rebelo, D. Orbanić, S. Chantepie, P. Contessotto, D. Papy-Garcia, C. Rodriguez-Cabello, M. Kilcoyne, K. Schenke-Layland, N. G. Karlsson, K. J. A. McCullagh, A. Pandit, *Biomaterials* **2021**, *269*, 120641.
[26] C. García-Arévalo, M. Pierna, A. Girotti, F. J. Arias, J. C. Rodríguez-Cabello, *Soft Matter* **2012**, *8*, 3239.
[27] T. Flora, I. González de Torre, M. Alonso, J. C. Rodríguez-Cabello, *Biofabrication* **2019**, *11*, 035008.
[28] F. González-Pérez, M. Alonso, I. González de Torre, M. Santos, J. C. Rodríguez-Cabello, *Adv. Healthcare Mater.* **2022**, *11*, 2201646.
[29] P. Contessotto, D. Orbanić, M. Da Costa, C. Jin, P. Owens, S. Chantepie, C. Chinello, J. Newell, F. Magni, D. Papy-Garcia, N. G. Karlsson, M. Kilcoyne, P. Dockery, J. C. Rodríguez-Cabello, A. Pandit, *Sci. Transl. Med.* **2021**, *13*, eaaz5380.
[30] A. Fernández-Colino, F. Wolf, S. Rütten, T. Schmitz-Rode, J. C. Rodríguez-Cabello, S. Jockenhoevel, P. Mela, *Frontiers in Bioengineering and Biotechnology* **2019**, *7*.
[31] N. T. Saidy, A. Fernández-Colino, B. S. Heidari, R. Kent, M. Vernon, O. Bas, S. Mulderrig, A. Lubig, J. C. Rodríguez-Cabello, B. Doyle, D. W. Hutmacher, E. M. De-Juan-Pardo, P. Mela, *Adv. Funct. Mater.* **2022**, *32*, 2110716.
[32] F. González-Pérez, S. Acosta, S. Rütten, C. Emonts, A. Kopp, H.-W. Henke, P. Bruners, T. Gries, J. C. Rodríguez-Cabello, S. Jockenhoevel, A. Fernández-Colino, *Frontiers in Bioengineering and Biotechnology* **2022**, *10*.
[33] K. Elkhoury, M. Morsink, L. Sanchez-Gonzalez, C. Kahn, A. Tamayol, E. Arab-Tehrany, *Bioactive Materials* **2021**, *6*, 3904.
[34] B. Aghaei-Ghareh-Bolagh, S. M. Mithieux, M. A. Hiob, Y. Wang, A. Chong, A. S. Weiss, *Acta Biomater.* **2019**, *91*, 112.
[35] B. Aghaei-Ghareh-Bolagh, S. Mukherjee, K. M. Lockley, S. M. Mithieux, Z. Wang, S. Emmerson, S. Darzi, C. E. Gargett, A. S. Weiss, *Materials today. Bio* **2020**, *8*, 100081.
[36] Q. L. Loh, C. Choong, *Tissue Eng., Part B* **2013**, *19*, 485.
[37] P. Yadav, G. Beniwal, K. K. Saxena, *Materials Today: Proceedings* **2021**, *44*, 2623.
[38] C. M. Murphy, M. G. Haugh, F. J. O'Brien, *Biomaterials* **2010**, *31*, 461.
[39] Z. Xu, W. Wen, T. Zhai, *Metall. Mater. Trans. A* **2012**, *43*, 2763.
[40] L. Debelle, A. J. P. Alix, *Biochimie* **1999**, *81*, 981.
[41] S. Roberts, M. Dzuricky, A. Chilkoti, *FEBS Lett.* **2015**, *589*, 2477.
[42] D. W. Urry, R. G. Shaw, K. U. Prasad, *Biochem. Biophys. Res. Commun.* **1985**, *130*, 50.
[43] T. Yamaoka, T. Tamura, Y. Seto, T. Tada, S. Kunugi, D. A. Tirrell, *Biomacromolecules* **2003**, *4*, 1680.
[44] C. Nicolini, R. Ravindra, B. Ludolph, R. Winter, *Biophys. J.* **2004**, *86*, 1385.
[45] S. E. Glassford, B. Byrne, S. G. Kazarian, *Biochimica et Biophysica Acta (BBA) – Proteins and Proteomics* **2013**, *1834*, 2849.
[46] E. S. Fioretta, S. E. Motta, V. Lintas, S. Loerakker, K. K. Parker, F. P. T. Baaijens, V. Falk, S. P. Hoerstrup, M. Y. Emmert, *Nat. Rev. Cardiol.* **2021**, *18*, 92.
[47] M. C. Gaspar, P. Coimbra, H. C. de Sousa, *Int. J. Pharm.* **2023**, *634*, 122671.
[48] P. Villard, M. Rezaeeyazdi, T. Colombani, K. Joshi-Navare, D. Rana, A. Memic, S. A. Bencherif, *Adv. Healthcare Mater.* **2019**, *8*, 1900679.
[49] in European Medicines Agency, **2019**.
[50] A. Memic, M. Rezaeeyazdi, P. Villard, Z. J. Rogers, T. Abdullah, T. Colombani, S. A. Bencherif, *Macromol. Mater. Eng.* **2020**, *305*, 1900824.
[51] R. Galante, T. J. A. Pinto, R. Colaço, A. P. Serro, *J. Biomed. Mater. Res., Part B* **2018**, *106*, 2472.
[52] E. Trimm, K. Red-Horse, *Nat. Rev. Cardiol.* **2023**, *20*, 197.
[53] a) J. C. Rose, D. B. Gehlen, T. Haraszti, J. Köhler, C. J. Licht, L. De Laporte, *Biomaterials* **2018**, *163*, 128; b) B. Trappmann, J. E. Gautrot, J. T. Connelly, D. G. T. Strange, Y. Li, M. L. Oyen, M. A. Cohen Stuart, H. Boehm, B. Li, V. Vogel, J. P. Spatz, F. M. Watt, W. T. S. Huck, *Nat. Mater.* **2012**, *11*, 642.
[54] L. Bernardi, C. Giampietro, V. Marina, M. Genta, E. Mazza, A. Ferrari, *Integrative Biology* **2018**, *10*, 527.
[55] T. A. Russo, D. Stoll, H. B. Nader, J. L. Dreyfuss, *Life Sci.* **2018**, *213*, 214.
[56] N. Chandra Sekar, S. Aguilera Suarez, N. Nguyen, A. Lai, P. Thurgood, Y. Zhou, C. Chheang, S. Needham, E. Pirogova, K. Peter, K. Khoshmanesh, S. Baratchi, *ACS Appl. Mater. Interfaces* **2023**, *15*, 4863.
[57] K. Nagayama, Y. Kimura, N. Makino, T. Matsumoto, *Am. J. Physiol.: Cell Physiol.* **2012**, *302*, C1469.
[58] M. Versaevel, T. Grevesse, S. Gabriele, *Nat. Commun.* **2012**, *3*, 671.
[59] R. Tudureanu, I. M. Handrea-Dragan, S. Boca, I. Botiz, *Int. J. Mol. Sci.* **2022**, *23*, 7731.
[60] D. E. Heath, J. J. Lannutti, S. L. Cooper, *J. Biomed. Mater. Res., Part A* **2010**, *94A*, 1195.
[61] R. Kaunas, S. Usami, S. Chien, *Cellular Signalling* **2006**, *18*, 1924.
[62] M. Moretti, A. Prina-Mello, A. J. Reid, V. Barron, P. J. Prendergast, *Materials in medicine* **2004**, *15*, 1159.

[63] H. Alkazemi, T. Huang, M. Mail, Z. Lokmic-Tomkins, D. E. Heath, A. J. O'Connor, *ACS Appl. Mater. Interfaces* **2023**, *15*, 34631.
[64] P. D. Venkatraman, in *Advanced Knitting Technology*, (Eds: S. Maity, S. Rana, P. Pandit, K. Singha), Woodhead Publishing, Sawston, UK **2022**.
[65] P. E. Dijkman, A. Driessen-Mol, L. Frese, S. P. Hoerstrup, F. P. T. Baaijens, *Biomaterials* **2012**, *33*, 4545.
[66] D. Potart, M. Gluais, A. Gaubert, N. Da Silva, M. Hourques, M. Sarrazin, J. Izotte, L. Mora Charrot, N. L'Heureux, *Acta Biomater.* **2023**, *166*, 133.
[67] T. N. McAllister, M. Maruszewski, S. A. Garrido, W. Wystrychowski, N. Dusserre, A. Marini, K. Zagalski, A. Fiorillo, H. Avila, X. Manglano, J. Antonelli, A. Kocher, M. Zembala, L. Cierpka, L. M. de la Fuente, N. L'Heureux, *Lancet* **2009**, *373*, 1440.
[68] L. Magnan, G. Labrunie, M. Fénelon, N. Dusserre, M.-P. Foulc, M. Lafourcade, I. Svahn, E. Gontier, J. H. Vélez V, T. N. McAllister, N. L'Heureux, *Acta Biomater.* **2020**, *105*, 111.
[69] J. H. Lawson, M. H. Glickman, M. Ilzecki, T. Jakimowicz, A. Jaroszynski, E. K. Peden, A. J. Pilgrim, H. L. Prichard, M. Guziewicz, S. Przywara, J. Szmidt, J. Turek, W. Witkiewicz, N. Zapotoczny, T. Zubilewicz, L. E. Niklason, *Lancet* **2016**, *387*, 2026.
[70] L. E. Niklason, J. H. Lawson, *Science* **2020**, *370*, eaaw8682.
[71] A. Fernández-Colino, F. Kiessling, I. Slabu, L. De Laporte, P. Akhyari, S. K. Nagel, J. Stingl, S. Reese, S. Jockenhoevel, *Adv. Healthcare Mater.* **2023**, *12*, 2300991.
[72] T. B. Wissing, V. Bonito, C. V. C. Bouten, A. I. P. M. Smits, *npj Regenerative Medicine* **2017**, *2*, 18.
[73] L. A. Bockeria, O. Svanidze, A. Kim, K. Shatalov, V. Makarenko, M. Cox, T. Carrel, *J. Thorac. Cardiovasc. Surg.* **2017**, *153*, 1542.
[74] S. de Valence, J.-C. Tille, D. Mugnai, W. Mrowczynski, R. Gurny, M. Möller, B. H. Walpoth, *Biomaterials* **2012**, *33*, 38.
[75] A. A. Seyhan, *Translational Medicine Communications* **2019**, *4*, 18.
[76] C. E. T. Stowell, Y. Wang, *Biomaterials* **2018**, *173*, 71.
[77] A. Liberski, N. Ayad, D. Wojciechowska, R. Kot, D. M. P. Vo, D. Aibibu, G. Hoffmann, C. Cherif, K. Grobelny-Mayer, M. Snycerski, H. Goldmann, *Biotechnol. Adv.* **2017**, *35*, 633.
[78] I. González de Torre, M. Santos, L. Quintanilla, A. Testera, M. Alonso, J. C. Rodríguez Cabello, *Acta Biomater.* **2014**, *10*, 2495.
[79] R. Moreira, T. Velz, N. Alves, V. N. Gesche, A. Malischewski, T. Schmitz-Rode, J. Frese, S. Jockenhoevel, P. Mela, *Tissue Eng., Part C* **2014**, *21*, 530.
[80] C. A. Schneider, W. S. Rasband, K. W. Eliceiri, *Nat. Methods*, *9*, 671.
[81] D. R. Stirling, M. J. Swain-Bowden, A. M. Lucas, A. E. Carpenter, B. A. Cimini, A. Goodman, *BMC Bioinformatics* **2021**, *22*, 433.